Geomechanics and Engineering, *Vol. 11, No. 2 (2016) 235-252*
DOI: http://dx.doi.org/10.12989/gae.2016.11.2.235

Ultimate lateral capacity of two dimensional plane strain rectangular pile in clay

Suraparb Keawsawasvong [a] and Boonchai Ukritchon[*]

Geotechnical Research Unit, Department of Civil Engineering, Faculty of Engineering, Chulalongkorn University, Bangkok, Thailand

(*Received May 13, 2015, Revised December 21, 2015, Accepted April 28, 2016*)

Abstract. This paper presents a new numerical solution of the ultimate lateral capacity of rectangular piles in clay. The two-dimensional plane strain finite element was employed to determine the limit load of this problem. A rectangular pile is subjected to purely lateral loading along either its major or minor axes. Complete parametric studies were performed for two dimensionless variables including: (1) the aspect ratios of rectangular piles were studied in the full range from plates to square piles loaded along either their major or minor axes; and (2) the adhesion factors between the soil-pile interface were studied in the complete range from smooth surfaces to rough surfaces. It was found that the dimensionless load factor of rectangular piles showed a highly non-linear function with the aspect ratio of piles and a slightly non-linear function with the adhesion factor at the soil-pile interface. In addition, the dimensionless load factor of rectangular piles loaded along the major axis was significantly higher than that loaded along the minor axis until it converged to the same value at square piles. The solutions of finite element analyses were verified with the finite element limit analysis for selected cases. The empirical equation of the dimensionless load factor of rectangular piles was also proposed based on the data of finite element analysis. Because of the plane strain condition of the top view section, results can be only applied to the full-flow failure mechanism around the pile for the prediction of limiting pressure at the deeper length of a very long pile with full tension interface that does not allow any separation at soil-pile interfaces.

Keywords: numerical analysis; plane strain; finite element; limit analysis; rectangular piles

1. Introduction

At present, the applied loads from superstructures on foundations are significantly large such as loads from large bridge structures or high-rise buildings. Recently, new cast-in-place pile construction technologies have been developed and are being employed to give more allowable pile loads than those in the past. Even though a cast-in-place-pile section is usually circular, a rectangular pile known as the barrette pile has also become more commonly used in practice as it offers a number of advantages. For example, rectangular piles can carry larger axial loads and higher moments than circular piles. Rectangular pile construction uses the same equipment as that used for diaphragm and cut-off walls. Furthermore, rectangular piles remove the need for pile caps. As a result, the piles can be extended upwards without change of shape to form a single pile

∗Corresponding author, Sc.D., Associate Professor, E-mail: boonchai.uk@gmail.com
[a] Research Assistant

http://www.techno-press.org/?journal=gae&subpage=7 ISSN: 2005-307X (Print), 2092-6219 (Online)

barrette-column system. A calculation of the ultimate lateral load of rectangular piles is important in practice in order to evaluate its stability or the factor of safety against lateral applied loads which are arisen from wave forces in the sea, wind loading or forces of earthquake actions. Those forces may result in damages and failures of structures if the lateral applied load is greater than the ultimate lateral capacity of rectangular piles.

In a real problem of laterally loaded piles, the ultimate lateral capacity of piles increases with depth from an initial low value at the ground surface to a maximum value at a certain depth and remains constant in the deeper length of pile. The limiting pressure at the deeper depth of pile corresponds to the full-flow failure mechanism around pile (e.g., Murff and Hamilton 1993), where the complete lateral translation of a pile at a certain depth from the ground surface essentially takes place under the plane strain condition. To achieve the full-flow mechanism, it is assumed that the length of a pile is very long, and hence the two-dimensional (2D) plane strain condition in the top view section is applicable. Therefore, this paper aims to determine the ultimate lateral capacity of rectangular piles, where the full-flow failure mechanism develops.

Laterally loaded piles were first studied by Broms (1964) based on the assumed slip line pattern. Ultimate lateral load per unit length of pile, or ultimate lateral resistance, was proposed for several sections. The geometrical sections of piles in Broms's studies included circular piles, rotated square piles and plate sections. In addition, the values of adhesion factor (α) at the soil-pile interface in his studies were only at $\alpha = 0$ (smooth surface) and $\alpha = 1$ (rough surface). The definition of adhesion factor is $\alpha = s_{ui}/s_u$, where s_{ui} is the undrained shear strength at the soil-pile interface and s_u is the undrained shear strength of surrounding soil. However, Broms (1964) did not study the influence of other values of adhesion factor on the ultimate lateral resistance on those sections.

Previous works of ultimate lateral capacity of piles mostly focused on circular sections. Randolph and Houlsby (1984) presented the two-dimensional lower bound and upper bound plastic calculations based the method of characteristics for circular piles in clay with adhesion factor in the range of 0 – 1. But their upper bound and lower bound solutions were not an exact solution for all adhesion factor cases. Subsequently, Martin and Randolph (2006) presented an improved upper bound solution, which is very closed to the lower bound solution of Randolph and Houlsby (1984) for the complete range of adhesion factor. In addition, Ukritchon (1998) presented a numerical solution for ultimate lateral load of a circular pile by the finite element limit analysis, which considered the effect of anisotropy in undrained shear strength. Recently, the finite element limit analysis was employed to solve the ultimate lateral load for problems encountered with two side-by-side circular piles with a symmetrical load (Georgiadis *et al*. 2013a), a row of circular piles (Georgiadis *et al*. 2013b), and two side-by-side circular piles with load inclination (Georgiadis *et al*. 2013c). However, their analyses did not provide solutions for the ultimate lateral load of rectangular piles.

In recent years, experimental studies of barrette piles have been performed. For example, Ho (1993), Ho and Lim (1996) and Ho and Tan (1998) gathered data of barrette pile load tests at many locations around the world. Their investigations included the relative pile displacement for the case of combined vertical and horizontal loads. In addition, they proposed empirical charts that estimated the adhesion factor related to N values or results of SPT testing. Plumbridge *et al*. (2000) presented testing results for barrette and circular piles, where both piles were subjected to lateral load for resisting the construction of railway tracks in Hong Kong. They proposed an equation for predicting pile displacement based on N values or results of SPT testing. In addition, there are other studies by experimental approaches for explaining behaviors of barrette pile such as

researches by Zhang (2003) and Raymond and Fan (2002). Finite element methods (e.g., Hsueh *et al*. 2014, Abbas *et al*. 2008 and Submaneewong 1999, 2009) were employed to analyze behaviors of barrette piles and to get empirical equations for explaining the behaviors of barrette piles, such as the load-displacement curves or the horizontal pile movement. However, all of those researches did not provide the ultimate lateral load of rectangular pile in form of dimensionless parameters.

Several classical foundation engineering books (e.g., Reese and Van Impe 2007, Poulos and Davis 1980, Randolph and Gourvenec 2011) do not provide any solution of ultimate lateral load of rectangular piles. Existing solutions of ultimate lateral capacity of piles appears only for circular section as described earlier. The effects of adhesion factor at soil-pile interface and aspect ratio of pile on the ultimate lateral capacity of rectangular piles have not been addressed before.

This paper presents a new numerical solution of the ultimate lateral capacity of rectangular piles in clay by finite element analyses. The 2D plane strain condition is assumed, and thus it is strictly applied for the full-flow failure mechanism of the ultimate lateral capacity of rectangular piles. The rectangular pile is subjected to purely lateral loading along either its major or minor axes. Complete parametric studies of the aspect ratio of the pile (B/H) and the adhesion factor (α) at the soil-pile interface were carried out by finite element analysis. Results were summarized in form of the dimensionless ultimate load factor of rectangular piles as a function of the aspect ratio of the pile and the adhesion factor at the soil-pile interface. Numerical solutions of dimensionless load factor of rectangular piles were verified by those of finite element limit analysis for some selected cases. A single empirical equation was also proposed for predicting the dimensionless load factor of rectangular piles in design practice.

2. Method of analysis

This paper employed the commercial finite element software, Plaxis 2D by Brinkgreve (Brinkgreve and Bakker 1991, Brinkgreve 2007) to determine the ultimate lateral capacity of rectangular piles in clay as shown in Fig. 1. It is assumed that the full-flow mechanism around the pile develops and the length of a rectangular pile is very long. Thus, small strain finite element models using the 2D plane strain condition in the top view section are setup to analyze the ultimate lateral capacity of rectangular pile loaded along either its major or minor axes. In the finite element analysis, the clay is modelled as the volume element with the Tresca material and the associated flow rule. Its parameters include the undrained shear strength (s_u), the undrained Young's modulus,

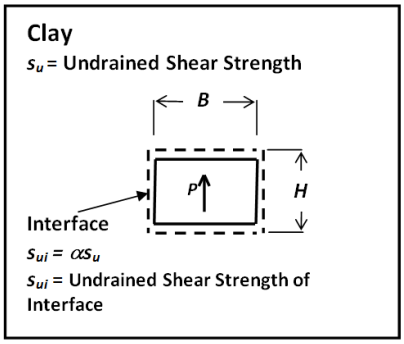

Fig. 1 Problem definition of ultimate lateral capacity of rectangular pile in clay

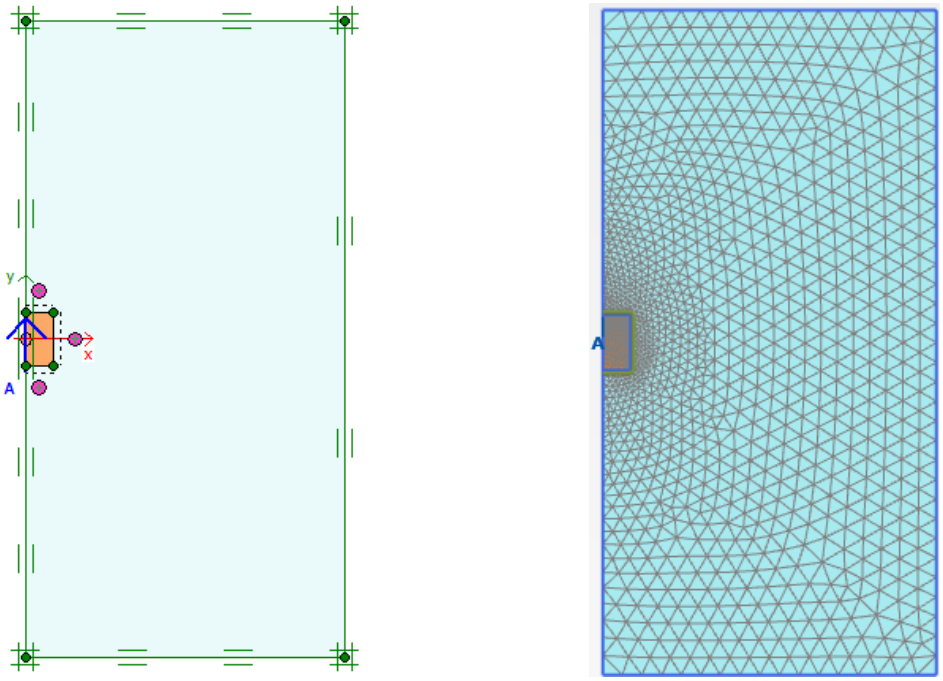

(a) (b)

Fig. 2 (a) Model geometry of rectangular pile; (b) typical mesh used in finite element analysis

$E_u = 500s_u$, Poisson's ratio (ν) = 0.495, the total friction angle (ϕ) = 0 and the total dilation angle (ψ) = 0. The ratio, E_u/s_u = 500 was selected based on a typical value commonly used by other studies of the finite element analysis to determine the limit load of geotechnical stability problems such as Georgiadis *et al.* (2013a, b, c). For stability problems, it is expected that the value of Young's modulus should not influence the limit load at the failure state for the soil obeying the linear elastic perfectly plastic material with the associated flow rule. The clay is defined as a weightless material or zero unit weight (i.e., $\gamma = 0$) for the assumption of plane strain condition in the top view section.

The geometry model is shown in Fig. 2(a). The rectangular pile is modelled as the volume element with the elastic properties of the concrete, where Poisson's ratio (ν) = 0.21, Young's modulus, $E_u = 2.9 \times 10^7$ kPa. The geometrical parameters of rectangular piles include the width (B) and the length (H), giving rise to the aspect ratio of the pile, B/H (or H/B). A rectangular pile is loaded by the force, P at the center along either its major or minor axes that correspond to the largest and smallest moments of inertia of their axes of symmetry. The pile aspect ratios, B/H are studied in the complete range as $0 - \infty$, namely, $B/H = 0 - 1$ and $H/B = 0 - 1$. For the case of $B/H < 1$, a rectangular pile is laterally loaded along its minor axis. In contrast, for the case of $H/B < 1$, a rectangular pile is laterally loaded along its major axis. The case of $H/B = 0$ corresponds to the plate loaded perpendicularly, but the case of $B/H = 0$ corresponds the plate loaded in parallel.

For the cases of $B/H \neq 0$ or $H/B \neq 0$, the piles are modelled as the volume element. On the other hand, the cases of $B/H = 0$ or $H/B = 0$ are modelled as the plate element with the elastic properties of concrete that are the same values of volume elements. Fig. 3 summarizes the modelling conditions of rectangular piles. The parametric study of those two extreme cases (i.e., $B/H = 0$ or

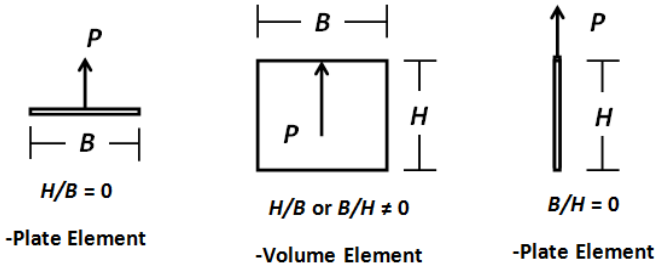

Fig. 3 Models of rectangular pile in the complete aspect ratio of the pile

H/B = 0) enables the complete development of a curve fitting equation for the ultimate lateral capacity of rectangular piles, which will be presented later.

Interface elements between the clay and the pile are used around the perimeter of rectangular piles. Adhesion factor (α) at the soil-pile interface is also studied in the range of 0 – 1 with the increment of 0.25. Because of the assumption of the full-flow mechanism, the interface elements are modeled as the full tension case.

Owing to the symmetry of the geometry, only half of the problem is analyzed. The top and bottom boundaries of the model are fixed vertically. The left and right boundaries of the model are fixed horizontally. Triangular types of volume elements are used for modeling clays and pile. There are 15 nodes for each triangular element, corresponding to the cubic strain element type. The interface elements have 10 nodes for each element. In addition, the very fine mesh distribution is setup in order to obtain accurate results of the limit state analysis. Fig. 2(b) shows an example of a typical finite element mesh of rectangular pile.

There are five dimensional parameters of the laterally loaded rectangular pile, namely P, s_u, s_{ui}, B, H, where P is the ultimate lateral load per unit length of pile. However, the dimensionless technique (Butterfield 1999) can decrease the number of parameters from five dimensional parameters to three dimensionless parameters, namely $P/s_u(B+H)$, $\alpha = s_{ui}/s_u$, H/B or B/H. The normalized form of the ultimate resistance of laterally loaded pile, $P/s_u(B+H)$, is one of the options of the dimensionless parameter which can be used for any general case including two extreme cases of H/B = 0 and B/H = 0. If either P/s_uB or P/s_uH is adopted as the dimensionless form of the ultimate resistance, this term cannot be evaluated mathematically when B = 0 or H = 0. Thus, the dimensionless load factor of rectangular piles is generalized to be a function of the aspect ratio of the pile (B/H or H/B) and the adhesion (α) at the soil-pile interface as

$$\frac{P}{s_u(B+H)} = f(\alpha, \frac{B}{H} or \frac{H}{B}) \tag{1}$$

Where, α = 0 – 1, and B/H = 0 – 1 and H/B = 0 – 1.

3. Results

Unique dimensionless parameters are verified numerically when the rectangular pile has constant input dimensionless parameters, α and B/H. Table 1 summarizes the numerical verification of uniqueness of dimensionless parameters of laterally loaded rectangular piles. The analyses are setup with different input values of dimensional parameters, but have the same input

Table 1 Verification of uniqueness of dimensionless parameters

No.	B	H	s_u	s_{ui}	P	B/H	α	$P/s_u(H+B)$
	(m)	(m)	(kN/m^2)	(kN/m^2)	(kN/m)	(-)	(-)	(-)
1	0.60	1.00	20.00	10.00	188.81	0.60	0.50	5.90
2	0.30	0.50	10.00	5.00	47.22	0.60	0.50	5.91
3	1.00	1.00	100.00	50.00	1435.87	1.00	0.50	7.18
4	2.00	2.00	80.00	40.00	2296.28	1.00	0.50	7.18
5	0.60	1.00	200.00	150.00	1998.42	0.60	0.75	6.25
6	0.30	0.50	100.00	75.00	499.84	0.60	0.75	6.25

dimensionless parameters. In addition, two ratios of B/H and α are selected in this numerical verification. As shown in Table 1, the ranges of s_u correspond to the typical values of undrained shear strength for soft clay (10, 20 kPa), medium clay (80, 100 kPa) and stiff clay (200 kPa), while the ranges of s_{ui} give rise to the adhesion factor, $\alpha = s_{ui}/s_u$, in between 0.5-1.0 which are typical values used in the design practice for calculations of single pile capacity. The corresponding values of the lateral limit load, P are the computed results from the finite element simulation with the input variables, B, H, s_u, s_{ui}. Then, the corresponding dimensionless load factor, $P/s_u(H+B)$ is calculated straightforwardly.

The cases of No.1 and No.2 have different values of the input dimensional parameters, B, H, s_u and s_{ui}, but they generate the same values of input dimensionless parameters, α and B/H. Even though both cases have different values of the ultimate lateral load, P, they have almost the same value of output dimensionless parameter, $P/s_u(H+B)$. From another two examples, the cases of No. 3 and No. 4 and the cases of No. 5 and No. 6 indicate that the output dimensionless parameters, $P/s_u(H+B)$ are unique when the input dimensionless parameters, α and B/H of each case are the same.

In addition, the comparisons between No. 1 and No. 3 and No. 1 and No. 5 show that the output dimensionless parameters, $P/s_u(H+B)$ depends on the input dimensionless parameters of B/H and α. Accordingly, it can be numerically verified that the output dimensionless parameter, $P/s_u(H+B)$ is a function of B/H and α, and is unique provided that each term of B/H and α is unique.

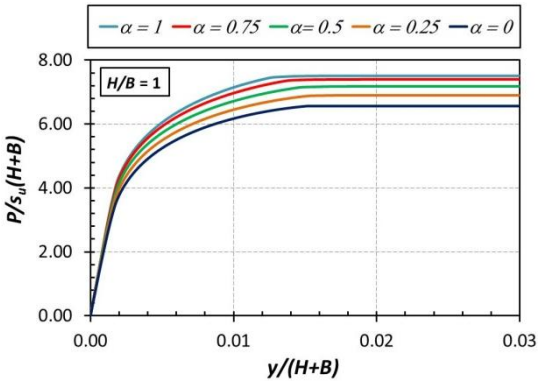

Fig. 4 Dimensionless load factor versus normalized displacement for H/B = 1, where, α = 0, 0.25, 0.5, 0.75 and 1

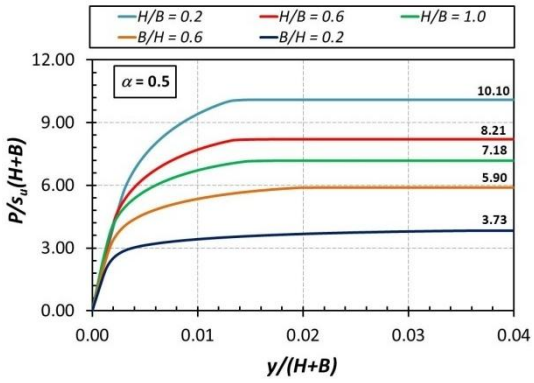

Fig. 5 Dimensionless load factor versus normalized displacement for α = 0.5, where, H/B = 0.2, 0.6, 1 and B/H = 0.6, 0.2

Figs. 4 and 5 show curves of the dimensionless load factor, $P/s_u(H+B)$ against the normalized displacement, $y/(H+B)$, where y is the displacement of rectangular pile in the same direction of the applied load. Fig. 4 shows cases of the same ratio of H/B = 1 with different adhesion factors, while Fig. 5 shows cases of the same ratio of α = 0.5, with different ratios of H/B. It can be observed that the limit state of all cases is successfully solved and obtained by the finite element analysis, where all the curves converge to a certain value for a very large displacement. In addition, it can be seen that a decrease of adhesion factor leads to the lower capacity of ultimate lateral resistance. In addition, an increase of H/B value results in the lower capacity of ultimate lateral resistance.

Figs. 6 and 7 show examples of failure mechanisms of laterally loaded rectangular pile obtained from finite element analyses. The failure mechanisms include the vector of incremental displacement (Fig. 6) and the incremental shear strain contour (Fig. 7). For those figures, results correspond with the same aspect ratio, H/B = 0.8, but have three different adhesion factors as α = 0, 0.5 and 1. It can be observed that the failure mechanism consists of two rigid triangular zones located on the front and back side of the pile and radial shear zone on both sides of the pile starting from the front of rigid triangular zone and ending at the back one. The radial shear zone joining corners of two triangular rigid zones appear like an ellipse. The size of radial shear zone depends on the adhesion factor and the aspect ratio of pile. In addition, there is some difference in the size of radial shear zone between smooth case (α = 0) and rough case (α = 1).

Figs. 8 and 9 compare failure mechanisms of rough piles which have different aspect ratios, B/H = 0.2, 1 and 5 (or H/B = 5, 1 0.2). Similar failure mechanisms can be observed in all cases.

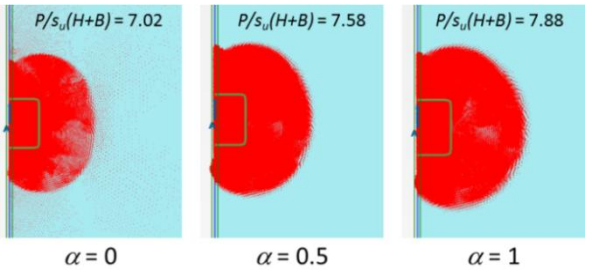

Fig. 6 Vector of incremental displacement (H/B = 0.8)

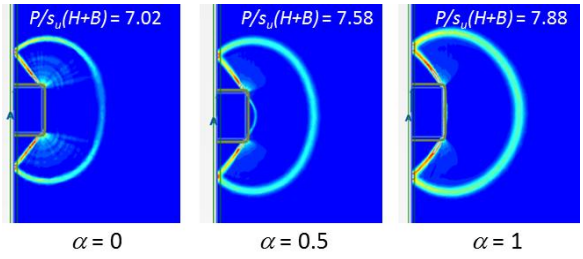

Fig. 7 Incremental shear strain contour (H/B = 0.8)

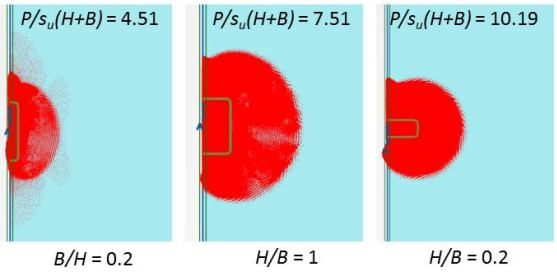

Fig. 8 Vector of incremental displacement (α = 1)

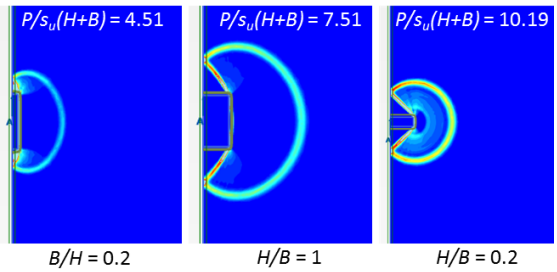

Fig. 9 Incremental shear strain contour (α = 1)

The size of failure zone also depends on B/H and reduces with the decrease in value of both B/H and H/B.

Fig. 10 shows the relationship between the dimensionless load factor, $P/s_u(H+B)$ and adhesion factor, α. In this figure, each line corresponds to the contour of H/B from 0 – ∞ (or B/H from ∞ – 0). In general, the dimensionless load factor increases with the increase in adhesion factor except the case of plate loaded perpendicularly (H/B = 0). The highest gradient of the curve correspond to the case of plate loaded in parallel (B/H = 0). A slightly nonlinear relationship between $P/s_u(H+B)$ and α is also observed for smaller value of B/H. The ultimate lateral capacity, $P/s_u(H+B)$ is constant of 11.538 regardless of the adhesion factor when the plate is loaded perpendicularly (H/B = 0). It should be noted that this solution corresponds very well with that of Merifield *et al*. (2001) who employed the finite element limit analysis (lower bound and upper bound methods) to compute the uplift capacity of deep and rough plate anchors in weightless clay as: P/s_uB = 10.28 – 11.42 (H = 0). Broms (1964) also obtained the solutions of this problem based on the assumed slip line field as: P/s_uB = 11.42 (at α = 0, smooth surface) and P/s_uB = 12.52 (at α = 1, rough surface).

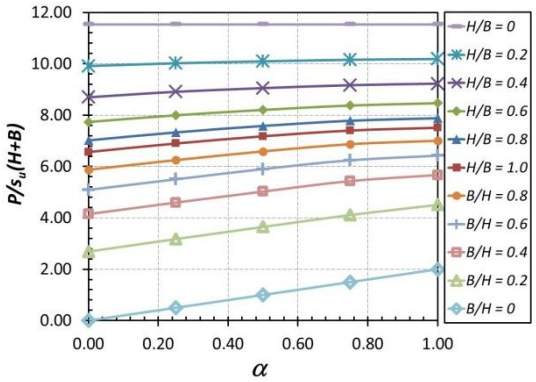

Fig. 10 Dimensionless load factor of rectangular piles versus adhesion factor

Thus, the comparisons suggest that the slip line field assumed by Broms (1964) is not correct for the exact solution of this special case. It is expected that his slip line solutions do not satisfy the complete requirements of the lower bound theorem, where the stress field is not statically admissible at the infinite domain of the problem.

For the plate loaded in parallel (B/H = 0), the failure load of this problem can be simply calculated using the static equilibrium of the force parallel to the plate. The failure load is obtained by integrating the interface shear resistance along two sides of the plate, resulting in the limit equilibrium solution as: $P/s_u(B+H) = 2\ \alpha$. It can be seen that the dimensionless load factor has a linear relationship with adhesion factor with the gradient of 2. This result agrees very well with the computed dimensionless load factor of the bottom contour line in Fig. 10, where the curve is the straight line with the gradient of 2 and passes the origin.

It should be noted that the lateral capacity of the square pile is (i.e., B/H=1): P/s_uB = 15.02 (rough) – 13.13 (smooth). The analytical solutions of the upper and lower bound values of circular piles reported by Martin and Randolph (2006) are: rough surface, P/s_uD = 11.94 (LB=UB); smooth surface, P/s_uD = 9.14 (LB) – 9.20 (UB), where D = the diameter of circular pile. Thus, this comparison indicates that the ultimate lateral capacity of square piles is larger than that of the circular piles about 25-40% depending on the adhesion factor at the soil-pile interface.

Figs. 11(a) and (b) show the relationship between the dimensionless load factor, $P/s_u(H+B)$ and the aspect ratio of pile, H/B and B/H, respectively. In this figure, each line in the graph corresponds to the contour of adhesion factor, α which ranges from 0 – 1. The bottom and top of the curves correspond to the cases of smooth surface (α = 0) and rough surface (α = 1), respectively. It should be noted that all curves converge to the same value of 11.538, which corresponds to the solution of the plate loaded perpendicularly, regardless of any value of adhesion factor. The influence of adhesion factor is very predominant when B/H = 0 – 1, but has small effect when H/B = 0 – 1. It can be observed that the dimensionless load factor, $P/s_u(H+B)$ has significant non-linear relationship with the aspect ratio of pile, H/B or B/H.

It should be noted that the finite element analyses were also performed for the models whose the soil-pile interfaces corresponded to the no tension case for several input values of B/H and α. It was found that the dimensionless load factor of rectangular piles for the cases of full tension and no tension at the soil-pile interface were the same for all selected values of those input parameters. This is because the unit weight of the soil is set to zero (i.e., weightless soil) due to the assumption of 2D plane strain condition in the top view section. Thus, a more realistic behavior of soil

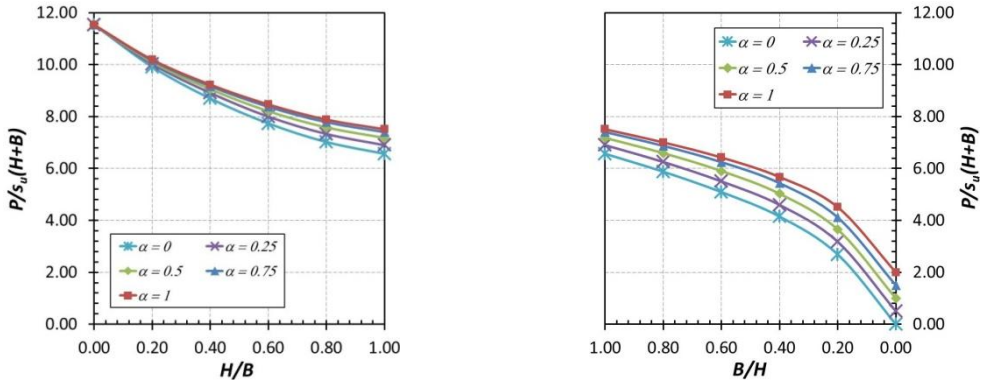

(a) (b)

Fig. 11 Dimensionless load factor of rectangular piles versus aspect ratio of pile, where: (a) H/B = 0 – 1; (b) B/H = 1 – 0

separating from the pile on the back side cannot be simulated using this simplified 2D model, which is the major limitation in the present study.

4. Verification of solutions by finite element limit analysis

The results of the present studies are verified by the state-of-the-art software, the finite element limit analysis (FELA), OptumG2 by Krabbenhoft *et al*. (2014). This software is the combination of limit analysis method and finite element method. OptumG2 was employed to determine the ultimate lateral capacity of rectangular piles using the upper bound method and the lower bound method. In addition, this software can perform mesh adaptively in order to obtain a more accurate lower bound and upper bound solutions (Lyamin *et al*. 2005 and Martin 2011). Numerical models of laterally loaded rectangular piles were analyzed by OptumG2 using the feature of mesh adaptively by starting from 5000 elements to 10000 elements in five adaptive iterations.

Material properties in OptumG2 simulations were the same as those of finite element analysis. In addition, boundaries conditions of OptumG2 models were also similar to those of finite element analysis. The distributed load in the OptumG2 simulation is applied at the top length of rectangular pile. The full tension condition at the soil-pile interface in OptumG2 was employed similarly as those in Plaxis. It should be noted that it is not necessary to verify the uniqueness of dimensionless parameters for OptumG2 since this verification was successfully carried out in the previous section such that the dimensionless load factor, $P/s_u(B+H)$ was numerically proved to be a unique function of B/H and α.

Fig. 12 shows the numerical model of rectangular pile in this verification, which are comprised of three different aspect ratios including B/H = 0.2, H/B = 1 and H/B = 0.2. These three cases have the same adhesion factor of rough surface, α = 1. The selection of these three cases is to compare failure mechanisms of OptumG2 with those of Plaxis as shown in Figs. 8 and 9. Triangular mesh of volume elements are used for modeling clay and pile. Fig. 13 shows the element types in OptumG2. For the lower bound analysis, there are three corner nodes of unknown stresses and stress discontinuities are permitted to occur at all shared edges of triangular elements including soil-pile interfaces. For the upper bound analysis, there are six corner nodes of unknown

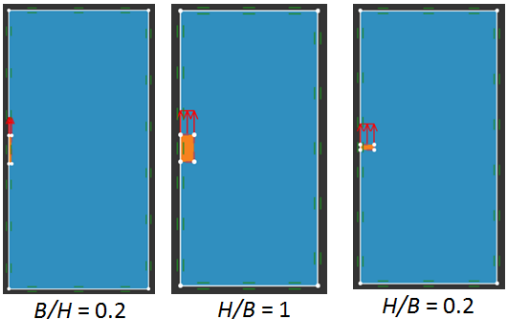

Fig. 12 Problem geometry of laterally loaded rectangular piles by OptumG2

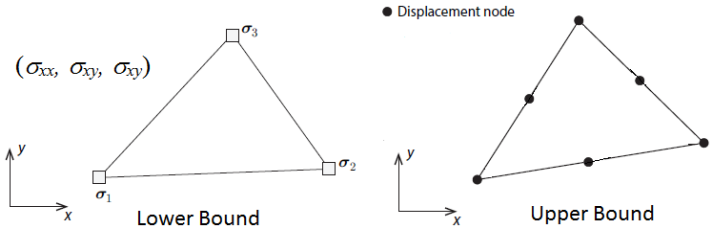

Fig. 13 Element types of lower bound and upper bound analyses in OptumG2

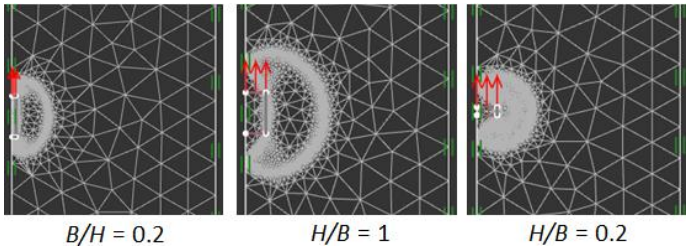

Fig. 14 Example of final adaptive meshes of laterally loaded rectangular piles by OptumG2 (α = 1)

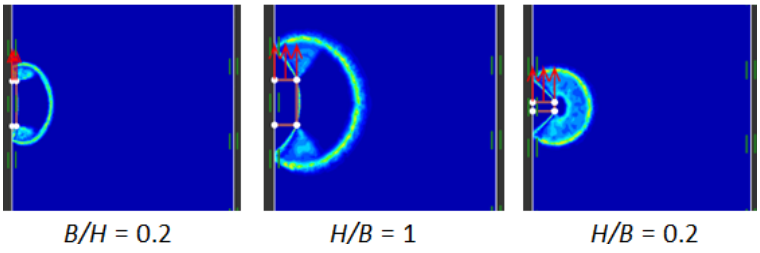

Fig. 15 Contours of incremental shear strain of laterally loaded rectangular piles by OptumG2 (α = 1)

displacement rate (velocity) and velocities discontinuities are permitted to occur only at soil-pile interfaces. The examples of final adaptive meshes are shown in Fig. 14. Fig. 15 shows the contour of incremental shear strain for three selected cases. It can be observed that the results of OptumG2 are comparable to those of the finite element analysis shown in Fig. 9.

Table 2 Verification of finite element solutions with finite element limit analysis solutions

No. (1)	B/H (2)	H/B (3)	α (4)	$P/s_u(H+B)$, FEA (5)	$P/s_u(H+B)$, UB (6)	$P/s_u(H+B)$, LB (7)	$P/s_u(H+B)$, Average (8) = [(6)+(7)]/2	% Difference (9) = [(5)-(8)]*100/(8)
1	0.2	5.0	0.0	2.64	2.55	2.43	2.49	5.53
2	0.2	5.0	0.5	3.65	3.54	3.43	3.48	4.57
3	0.2	5.0	1.0	4.51	4.47	4.30	4.39	2.72
4	1.0	1.0	0.0	6.57	6.40	6.13	6.27	4.55
5	1.0	1.0	0.5	7.18	7.10	6.82	6.96	3.08
6	1.0	1.0	1.0	7.51	7.49	7.27	7.38	1.75
7	5.0	0.2	0.0	9.91	9.90	9.56	9.73	1.89
8	5.0	0.2	0.5	10.10	10.10	9.74	9.92	1.74
9	5.0	0.2	1.0	10.19	10.19	9.91	10.05	1.40

Table 2 shows some examples of the upper bound and the lower bound solutions analyzed by OptumG2. The upper bound solutions shown in column 6 and the lower bound solutions shown in column 7 are averaged to give the average solutions in column 8. From a theoretical point of view, the exact solution is well approximated using the average of LB and UB, while the LB solution is more important in practice since it is always a safe solution. Since the differences between the computed LB and UB solutions in Table 2 were small, finite element solutions in column 5 were compared with the average of UB and LB solutions in column 8 giving rise to the percentage difference in column 9. It can be seen that there are good and rational agreements between the two solutions, where the differences range between 1 – 5.5%.

Large difference between Plaxis and OptumG2 happen when $B/H = 0.2$ and $\alpha \leq 0.5$ because the meshes used in the finite element analysis are not refined enough in the zone of high degree of shearing along the perimeter of piles. However, accurate quantitative agreements between FEA and OptumG2 can be generally achieved for all selected values of B/H and α. In particular, excellent agreement between Plaxis and OptumG2 can be observed at the square pile with fully rough surface (i.e., $B/H = 1$, $\alpha = 1$) and when $B/H = 5$ and $\alpha = 0 – 1$.

It should be noted that a finite element solution cannot be theoretically classified neither the lower bound solution nor the upper bound solution as extensively described in the state-of-the-art paper, geotechnical stability analysis by Sloan (2013). Not surprisingly, finite element solutions in Table 2 are higher than UB solutions by OptumG2. However, small differences between two solutions can be observed.

5. Development of the curve fitting equation of ultimate lateral capacity of rectangular piles

This section presents the development of the curve fitting equation of ultimate lateral capacity of rectangular piles. For this problem, the ultimate load, P depends on four dimensional variables including B, H, s_u and s_{ui}. According to Table 1 of numerical verification of uniqueness, the dimensionless load factor of rectangular piles is a function of two independent dimensionless variables as follows

$$y = f(x_1, x_2) \tag{2}$$

Where, $y = P/s_u(H+B)$; Dimensionless load factor
$x_1 = \alpha = s_{ui}/s_u$; Adhesion factor
$x_2 = B/H$; Aspect ratio of rectangular pile

It should be noted that the case of $x_2 = 0$ corresponds to the plate loaded in parallel. On the other hand, the case of $x_2 = \infty$ corresponds to the plate loaded perpendicularly. The rough and smooth surface cases correspond to $x_1 = 1$ and $x_1 = 0$, respectively. The case of $x_2 = \infty$ may pose a problem for a simple mathematical function since it may not compute the function value at this limit.

In order to develop the curve fitting equation of laterally loaded rectangular piles, parametric studies of dimensionless parameters, x_1 and x_2, were carried out with the complete range of x_1 and x_2 as: 1) $x_1 = 0$, 0.25, 0.5, 0.75 and 1; and 2) $x_2 = 0$, 0.2, 0.4, 0.6, 0.8, 1, 1.25, 1.67, 2.5, 5 and ∞, where the results are shown in Figs. 10 and 11. Thus, there are fifty five data obtained from the finite element analysis for developing the empirical equation of ultimate lateral capacity of rectangular piles.

It can be observed from Figs. 10 and 11 that the dimensionless load factor is non-linear relationship with two independent dimensionless parameters, B/H and α. Generally, the non-linear polynomial of biquadratic function (e.g., Sauer 2014) is one of the effective functions which can be used in the curve fitting method as shown in Eq. (3).

$$y(x_1, x_2) = \sum_{i=0}^{2} \sum_{j=0}^{2} a_{ij} x^i y^j \tag{3}$$

However, this function cannot be applied to the special case, where x_2 approaches to infinity because y cannot be mathematically evaluated. Thus, the rational function which is created from this non-linear polynomial function is proposed in order to give a single expression which can handle the complete range of $x_2 = 0$ to ∞. The empirical rational function is proposed as shown in Eq. (4).

$$y(x_1, x_2) = \frac{A_1 x_1^2 x_2^2 + A_2 x_1 x_2^2 + A_3 x_1^2 x_2 + A_4 x_2^2 + A_5 x_1 x_2 + A_6 x_1^2 + A_7 x_2 + A_8 x_1 + A_9}{A_{10} x_1^2 x_2^2 + A_{11} x_1 x_2^2 + A_{12} x_1^2 x_2 + A_{13} x_2^2 + A_{14} x_1 x_2 + A_{15} x_{15}^2 + A_{16} x_2 + A_{17} x_1 + 1} \tag{4}$$

Where, y = Dimensionless load factor
x_1 = Adhesion factor
x_2 = Aspect ratio of rectangular piles
$A_1 - A_{17}$ = Constant coefficients

In the case of $x_2 = \infty$, Eq. (4) can be evaluated mathematically by taking the limit of a function at $x_2 = \infty$. Thus, when $x_2 = \infty$, the dimensionless load factor is shown in Eq. (5).

$$\lim_{x_2 \to \infty} y = \frac{A_1 x_1^2 + A_2 x_1 + A_4}{A_{10} x_1^2 + A_{11} x_1 + A_{13}} \tag{5}$$

From Eq. (4), there are seventeen empirical constants, $A_1 - A_{17}$. However, there are some inter-relationships among those constants by observing the results of finite element analysis. Thus, constraints among empirical constants must be setup in order to reduce the equation into a more

simple form. From Figs. 10 and 11, when $x_2 = \infty$ which is the plate loaded perpendicularly, the values of y is a constant of 11.538 for all values of $x_1 = 0 - 1$. Therefore, some inter-relationship must be enforced as follows: $A_1 = A_{18}A_{10}$, $A_2 = A_{18}A_{11}$, $A_4 = A_{18}A_{13}$, $A_{18} = 11.538$.

Accordingly, Eq. (5) can be reduced as shown in Eq. (6).

$$\lim_{x_2 \to \infty} y = A_{18}\left(\frac{A_{10}x_1^2 + A_{11}x_1 + A_{13}}{A_{10}x_1^2 + A_{11}x_1 + A_{13}}\right) = 11.538 \tag{6}$$

Where, A_{18} = Constant coefficient = 11.538

In the case of $x_2 = 0$ (the plate is loaded in parallel, $B/H = 0$), the solution can be calculated manually using the static equilibrium as described previously as: $y = P/s_uH = 2 \quad = 2x_1$. Therefore, when x_1 is equal to 0, 0.25, 0.5, 0.75 and 1, y is equal to 0, 0.5, 1, 1.5 and 2. Thus, additional constraints can be generated by considering each of those cases, where $x_2 = 0$ and $x_1 = 0 - 1$.

Substituting $x_1 = 0$, $x_2 = 0$ and $y = 0$, the Eq. (4) is as follows

$$y(0,0) = A_9 = 0 \tag{7}$$

Substituting $x_1 = 0.25$, $x_2 = 0$ and $y = 0.5$, the Eq. (4) is as follows

$$y(0.25,0) = \frac{A_9 + 0.25A_8 + 0.0625A_6}{0.25A_{17} + A_{15} + 1} = 0.5 \tag{8}$$

Substituting $x_1 = 0.5$, $x_2 = 0$ and $y = 1$, the Eq. (4) is as follows

$$y(0.5,0) = \frac{A_9 + 0.5A_8 + 0.25A_6}{0.5A_{17} + 0.25A_{15} + 1} = 1 \tag{9}$$

Substituting $x_1 = 0.75$, $x_2 = 0$ and $y = 1.5$, the Eq. (4) is as follows

$$y(0.75,0) = \frac{A_9 + 0.75A_8 + 0.5625A_6}{0.75A_{17} + 0.5625A_{15} + 1} = 1.5 \tag{10}$$

Substituting $x_1 = 1$, $x_2 = 0$ and $y = 2$, the Eq. (4) is as follows

$$y(1,0) = \frac{A_9 + A_8 + A_6}{A_{17} + A_{15} + 1} = 2 \tag{11}$$

It can be observed that there are five unknown parameters, namely A_6, A_8, A_9, A_{15} and A_{17}, which is involved with five constraints, Eqs. (7)-(11). Thus, the solution of this system of equation gives rise to: $A_6 = 0$, $A_8 = 2$, $A_9 = 0$, $A_{15} = 0$ and $A_{17} = 0$. Substituting results of A_6, A_8, A_9, A_{15} and A_{17} in Eq. (4), the final form of the proposal rational function is given as

$$y(x_1,x_2) = \frac{A_{18}A_{10}x_1^2x_2^2 + A_{18}A_{11}x_1x_2^2 + A_3x_1^2x_2 + A_{18}A_{13}x_2^2 + A_5x_1x_2 + A_7x_2 + 2x_1}{A_{10}x_1^2x_2^2 + A_{11}x_1x_2^2 + A_{12}x_1^2x_2 + A_{13}x_2^2 + A_{14}x_1x_2 + A_{16}x_2 + 1} \tag{12}$$

The Eq. (12) can be rewritten with new constant coefficient as follows

$$y(x_1,x_2) = \frac{C_1x_1^2x_2^2 + C_2x_1x_2^2 + C_3x_1^2x_2 + C_4x_2^2 + C_5x_1x_2 + C_6x_2 + 2x_1}{C_7x_1^2x_2^2 + C_8x_1x_2^2 + C_9x_1^2x_2 + C_{10}x_2^2 + C_{11}x_1x_2 + C_{12}x_2 + 1} \tag{13}$$

Where $C_1 - C_{12}$ = New constant coefficients

The relationships between each coefficient are: $C_1 = A_{18}C_7$, $C_2 = A_{18}C_8$, $C_4 = A_{18}C_3$, $C_1C_2 = C_7C_8$, $C_1C_4 = C_7C_3$, $C_2C_4 = C_8C_3$, and $A_{18} = 11.538$.

A statistical approach of curve fitting (e.g., Walpole *et al*. 2002) is applied to determine twelve empirical constants of the proposed empirical equation. In this approach, the nonlinear least square method is employed to find the most appropriate values of C_1 to C_{12} by the following equations as

$$Minimize(error^2) = Minimize(\sum_{i=1}^{n}(y_i - f_i)^2) \tag{14}$$

Where, f_i = Solutions from finite element analysis
y_i = Solutions from Eq. (13)
n = Number of data = 55

The technique of curve fitting leads to the least square type problem, where the residual sum of squares between the data and the corresponding prediction is minimized. The final result of the optimal set of twelve constants by the least square optimization problem is summarized in Table 3.

In statistic, the coefficient of determination, R^2 is the ratio that indicates how well the data fit in the statistical model, and it can be calculated by the following equations as

$$R^2 = 1 - \frac{SS_{res}}{SS_{tot}} \tag{15}$$

Where, $SS_{tot} = \sum_{i=1}^{n}(y_i - \bar{y})^2$

$SS_{res} = \sum_{i=1}^{n}(y_i - f_i)^2$

$\bar{y} = \frac{1}{n}\sum_{i=1}^{n} y_i$

In general, the value of the coefficient of determination is between 0 and 100%. The closer R^2 of 100%, the better fit of the model. Fig. 16 shows the comparison of dimensionless load factor between the proposed Eq. (13) and the finite element analysis. It can be seen that the dimensionless load factor of the proposed equation corresponds very well with those of finite element analysis, where the coefficient of determination, R^2 is very high of 99.99%.

Based on the proposed empirical equation, several special interesting cases can be computed as follows:

Substituting, $x_1 = 0$, $x_1 = 1$ into Eq. (13), the empirical equations of ultimate lateral capacity of rectangular piles for smooth and rough surfaces are:

Smooth surface of rectangular piles

$$\frac{P}{s_u(B+H)} = \frac{77.213(\frac{B}{H})^2 + 21.974(\frac{B}{H})}{6.692(\frac{B}{H})^2 + 7.613\left(\frac{B}{H}\right) + 1} \tag{16}$$

Rough surface of rectangular piles

Table 3 Optimal value of empirical constants

C_1	C_2	C_3	C_4	C_5	C_6	C_7	C_8	C_9	C_{10}	C_{11}	C_{12}
29.976	-35.775	4.432	77.213	12.935	21.974	2.598	-3.101	3.454	6.692	6.692	7.613

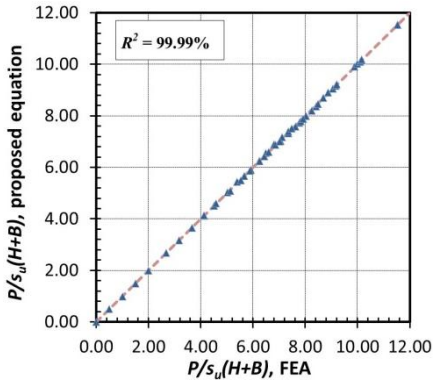

Fig. 16 Dimensionless load factor of the proposed equation versus that of finite element

$$\frac{P}{s_u(B+H)} = \frac{71.414(\frac{B}{H})^2 + 39.341\left(\frac{B}{H}\right) + 2}{6.190(\frac{B}{H})^2 + 7.896\left(\frac{B}{H}\right) + 1} \tag{17}$$

Substituting, x_2 = 1 into Eq. (13), the empirical equation of ultimate lateral capacity of square piles ($B = H$, $B/H = 1$) is

Square piles

$$\frac{P}{s_u B} = \frac{64.816(\alpha)^2 - 41.680(\alpha) + 198.372}{6.052(\alpha)^2 - 6.271(\alpha) + 15.305} \tag{18}$$

6. Conclusions

This paper presents a parametric study of ultimate lateral capacity of rectangular piles in clay where the full-flow failure mechanism develops. The two dimensional plane strain finite element was employed to determine stability of this problem. A rectangular pile is subjected to purely lateral loading along either its major or minor axes. The dimensionless load factor of rectangular piles, $P/s_u(H+B)$ is a function of the aspect ratio of the pile (B/H) and the adhesion factor (α at the soil-pile interface. The dimensionless load factor was validated numerically to have the unique value when the input dimensionless variables α, B/H are the same. In addition, typical curves of the dimensionless load factor against the normalized displacement were shown in this paper. It can be observed that the limit state of all selected cases was successfully solved and obtained by the finite element analysis, where all the curves converge to a certain value for a very large displacement. The dimensionless load factor has slightly nonlinear increasing function of adhesion factor, but has highly nonlinear decreasing function of H/B. The dimensionless load factor of rectangular piles loaded along the major axis was significantly higher than that loaded along the minor axis until it converged to the same value at square piles. Failure mechanisms of laterally

loaded rectangular piles were also postulated from this study, which depends on the adhesion factor at the soil-pile interface and the aspect ratio of the pile.

The results of the present studies were verified by the state-of-the-art software, finite element limit analysis (FELA), OptumG2 by Krabbenhoft *et al*. (2014). The average solutions of the upper bound and lower bound methods and the solutions of finite element analysis corresponded well and rationally with each other. A single empirical equation was proposed for a rapid and accurate prediction of the ultimate lateral capacity of rectangular piles in design practice. Specific applications and limitations of such predictions are related to the full-flow failure mechanism around pile, where predicted limiting pressure is not affected from the ground surface and can only be applicable for the deeper length of a very long pile. In addition, the results are only valid for the full tension case at the soil-pile interface where there is no separation at soil-pile interfaces.

References

Abbas, J.M., Chik, Z.H. and Taha, M.R. (2008), "Single pile simulation and analysis subjected to lateral load", *Electronic J. Geotech. Eng.*, **13**, 1-15.

Brinkgreve, R.B.J. (2007), *PLAXIS 2D, Version 8.5 finite-element code for soil and rock analyses: Complete set of manuals*, (R. Brinkgreve Ed.), Balkema, Rotterdam, The Netherlands.

Brinkgreve, R.B.J. and Bakker, H.L. (1991), "Non-linear finite element analysis of safety factors", *In Proceedings of the 7th International Conference on Computational Methods and Advances in Geomechanics*, Cairns, Australia, May.

Broms, B.B. (1964), "Lateral resistance of piles in cohesive soils", *J. Soil Mech. Found.*, **90**(2), 27-63.

Butterfield, R. (2009), "Dimensional analysis for geotechnical engineering", *Géotechnique*, **49**(2), 357-366.

Georgiadis, K., Sloan, S.W. and Lyamin, A.V. (2013a), "Ultimate lateral pressure of two side-by-side piles in clay", *Géotechnique*, **63**(9), 733-745.

Georgiadis, K., Sloan, S.W. and Lyamin, A.V. (2013b), "Undrained limiting lateral soil pressure on a row of piles", *Comput. Geotech.*, **54**, 175-184.

Georgiadis, K., Sloan, S.W. and Lyamin, A.V. (2013c), "Effect of loading direction on the ultimate lateral soil pressure of two piles in clay", *Géotechnique*, **63**(13), 1170-1175.

Ho, C.E. (1993), "Deep barrette foundation in Singapore weathered granite", *Proceedings of II the Southeast Asian Geotechnical Conference*, Singapore, May.

Ho, C.E. and Lim, C.H. (1996), "Barrette foundation constructed under polymer slurry support in old alluvium", *Proceedings of the 12th Southeast Asian Geotechnical Conference*, Kuala Lumpur, Malaysia, May.

Ho, C.E. and Tan, C.G. (1998), "Barrettes designed as friction foundations: a case history", *Proceedings of the 4th International Conference on Case Histories in Geotechnical Engineering*, St. Louis, MO, USA, March.

Hsueh, C.K., Lin, S.S. and Chen, S.G. (2004), "Lateral performance of drilled shaft considering nonlinear soil and structure material behavior", *J. Marine Sci. Technol.*, **12**(1), 62-71.

Krabbenhoft, K., Lyamin, A. and Krabbenhoft, J. (2014), *Optum Computational Engineering, Version 1.14: Manual*, OptumCE, Copenhagen, Denmark.

Lyamin, A., Sloan, S.W., Krabbenhoft, K. and Hjiaj, M. (2005), "Lower bound limit analysis with adaptive remeshing", *Int. J. Numer. Method. Eng.*, **63**(14), 1961-1974.

Martin, C.M. (2011), "The use of adaptive finite element limit analysis to reveal slip-line fields", *Geotech. Lett.*, **1**(2), 23-29.

Martin, C.M. and Randolph, M.F. (2006), "Upper-bound analysis of lateral pile capacity in cohesive soil", *Géotechnique*, **56**(2), 141-145.

Merifield, R.S., Sloan, S.W. and Yu, H.S. (2001), "Stability of plate anchors in undrained clay", *Géotechnique*, **51**(2), 141-153.

Murff, J.D. and Hamilton, J.M. (1993), "P-Ultimate for undrained analysis of laterally loaded piles", *J. Geotech. Eng.*, **119**(1), 91-107.
Plumbridge, G.D., Sze, J.W.C. and Tram, T.T.F. (2000), "Full scale lateral load tests on bored piles and a barrette", *Proceedings of the 19th Annual Seminar of Geotechnical Division*, Hong Kong, May.
Poulos, H.G. and Davis, E.H. (1980), *Pile Foundation Analysis and Design*, John Wiley & Sons, USA.
Randolph, M. and Gourvenec, S. (2011), *Offshore Geotechnical Engineering*, Spon Press, USA.
Randolph, M.F. and Houlsby, G.T. (1984), "The limiting pressure on circular pile loaded laterally in cohesive soil", *Géotechnique*, **34**(4), 613-623.
Raymond, J.C. and Fan, K. (2002), "Lateral load test results on drill shafts in Marl at Jacksonville", *Proceedings of the International Deep Foundations Congress*, Orlando, FL, USA, February.
Reese, L.C. and Van Impe, W.F. (2007), *Single Piles and Pile Groups under Lateral Loading*, Taylor & Francis Group plc, London, UK.
Sauer, T. (2014), *Numerical Analysis*, Pearson Education Limited, UK.
Sloan, S.W. (2013), "Geotechnical stability analysis", *Géotechnique*, 63(7), 531-572.
Submaneewong, C. (1999), "Behavior of Instrumented Barrette and Bored Pile in Bangkok Subsoils", Master's Thesis; Chulalongkorn University, Thailand.
Submaneewong, C. (2009), "Behavior of Vertical and Lateral Load on T-Shape Barrette and Bored Piles", Ph.D. Thesis; Chulalongkorn University, Thailand.
Ukritchon, B. (1998), "Application of numerical limit analyses for undrained stability problems in clay", Sc.D. Thesis; Massachusetts Institute of Technology, USA.
Walpole, R.E., Myers, R.H., Myers, S.L. and Ye, K. (2002), *Probability & Statistics for Engineering and Scientists*, (7th Ed.), Prentice Hall, NJ, USA.
Zhang, L.M. (2003), "Behavior of laterally loaded large-section barrettes", *J. Geotech. Geoenviron. Eng.*, **129**(7), 639-648.

CC